Introduction

Understanding the behavior of brine evaporation in fractured porous media under CO_2 gas injection is critical for various geological site and engineering applications, including carbon storage, enhanced geothermal systems, and hydrocarbon recovery. During gas injection process into a saline reservoir, pressure gradually increases, and overpressure in the subsurface can cause fractures, potentially leading to serious issues such as gas leakage [1,2]. As gas flows through the fracture in saline reservoir, brine evaporates, leading to salt precipitation. In some cases, the deposited salt may contribute to self-sealing fractures, reducing permeability and modifying fluid transport properties [3,4]. Such self-healing mechanisms could be beneficial for applications such as CO_2 sequestration, where containment integrity is crucial.

In porous media systems, capillary backflow occurs when brine redistributes due to pressure differences, ultimately leading to an advection-dominated flow. The evaporation process generates gradients concentration, driving diffusion. Simultaneously, the evaporation process creates pressure gradient due to the formation of menisci at the liquid-gas interfaces, which induce capillary pressure differences. These pressure gradients generate capillary backflow, acting as advection [5–7].
The Peclet number (Pe) is used to quantify the relative contribution of advection and diffusion. The interplay of diffusion and advection in the evaporation process ultimately determines whether salt accumulates or precipitates in the residual brine phase [8–10]. Investigating the evaporation process in fractured porous media will help clarify the overall understanding of brine evaporation and salt precipitation mechanisms.

To further understand these processes, it is essential to use X-ray microtomography for measuring brine saturation and concentration inside the porous structure. This imaging technique enables non-destructive, high-resolution visualization of fluid distribution within the system, allowing for precise quantification of saturation changes and salt deposition over time[6,11,12]. By employing X-ray microtomography, this study aims to capture detailed insights into the interactions between evaporation, advection, and diffusion, ultimately contributing to the improved management of fractured porous media.

Experimental Setup and Procedures

Three-dimensional experiments on the brine drying process via gas injection in a fractured porous medium were conducted using the experimental setup show in Fig. 1. A cylindrical column with an outer diameter of 14 mm and an inner diameter of 10 mm was packed with three layers of water-wet glass bead particles (As One, BZ-O6): 400 μm particles on both sides, with 1000 μm particles in the middle acting as the fracture zone. The packed bed consists of three parts: the top part serves as an injection point, the bottom part serves as an outlet, and the separate water tank is only connected to the 400 μm particles near the outlet with maximum capacity 4 cm^3 for each side. The packed bed parts were molded using a formlabs 3D printer [13].

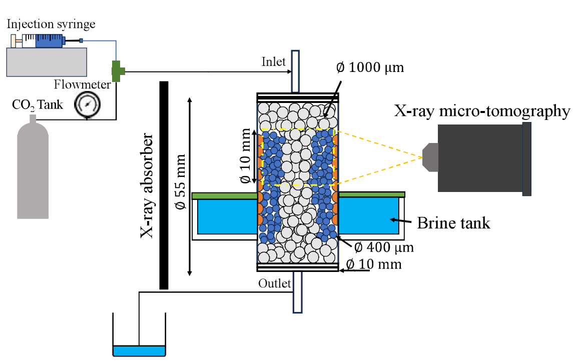

Fig. 1 Experimental setup

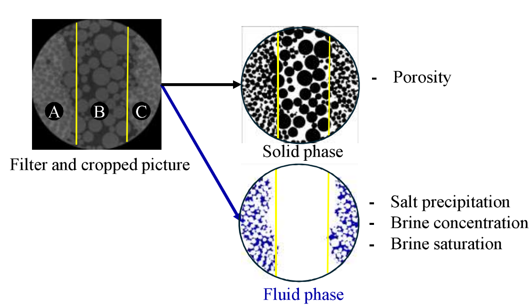

Fig. 2 Phase segmentation

The micro-CT scanner (Comscantechno, ScanXmate-CF110TSS300) was used to observe brine distribution in the packed bed until evaporation was complete. CO2 gas was injected as the displacement gas, and a NaI solution with 20 wt% salinity was used to differentiate gas, particles, and brine phases based on their distinct CT values. The brine concentration was estimated from CT values using a calibration curve derived from preliminary experiments. The experiment was conducted at a controlled room temperature of approximately 20°C, with the NaI solution's solubility limit at 64 wt%.

Glass beads were packed into three distinct layers within the container using a separator to ensure uniform packing density. Afterward, NaI solution was injected into both brine tanks using a syringe, and the tanks were sealed. Air within the porous media was removed using a vacuum chamber until full saturation was achieved. The packed bed was scanned using X-ray settings of 100 kV and 100 µA, with a voxel size of 10 µm/pixel, focusing on the fracture zone (Fig. 1). CO2 gas was injected initially at 25 ml/min (30 ml volume) and continuously afterward at 50 ml/min, with Reynolds numbers ranging from 10 to 88. During scanning, gas injection was paused, and each scan required about 40 minutes. The data set was reconstructed and processed using beam hardening, ring artifact, median, and denoise filters to enhance image quality. The packed bed was divided into three regions, with the fracture zone in the middle. Phase segmentation was performed to evaluate brine saturation and concentration, as illustrated in Fig. 2.

Result and discussion

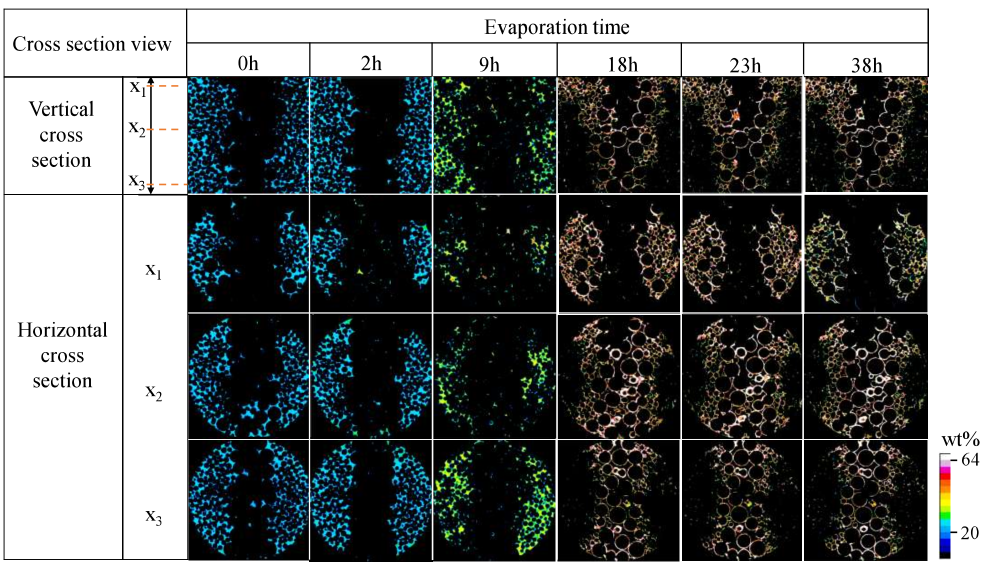

Fig. 3 Brine visualization and salt precipitation process

Fig. 3 illustrates the vertical and horizontal cross-sectional images of brine evaporation within fracture porous media, with the inlet located at the top. The color scale represents the brine concentration, where water evaporates, leaving behind salt. The top image shows the vertical cross-section, while the three bottom images represent horizontal cross-sections at x_1, x_2, and x_3. Evaporation halts when brine saturation and concentration stabilize. The porosity for three regimes was initially measured as 0.39±0.03, 0.31±0.03, and 0.39±0.02. Initially, the water occupied smaller pores due to higher capillary forces, while gas flowed through the fracture zone. Brine concentration remained uniform from top to bottom, as observed in the x_1 and x_3 cross-sections.

As evaporation progressed, brine saturation and concentration still stabilized even after 2 hours injection. The brine saturation started to decrease significantly after 9 hours, with the reduction appearing uniformly from top to bottom. Brine concentration increased, but this change was also uniform vertically. After 18 hours, brine reached the solubility limit (as shown by the white color) and began to form salt. Salt saturation increased near the inlet and at the interface between large and small particles. From 18 to 23 hours, brine saturation stabilized, although gas continued to penetrate.

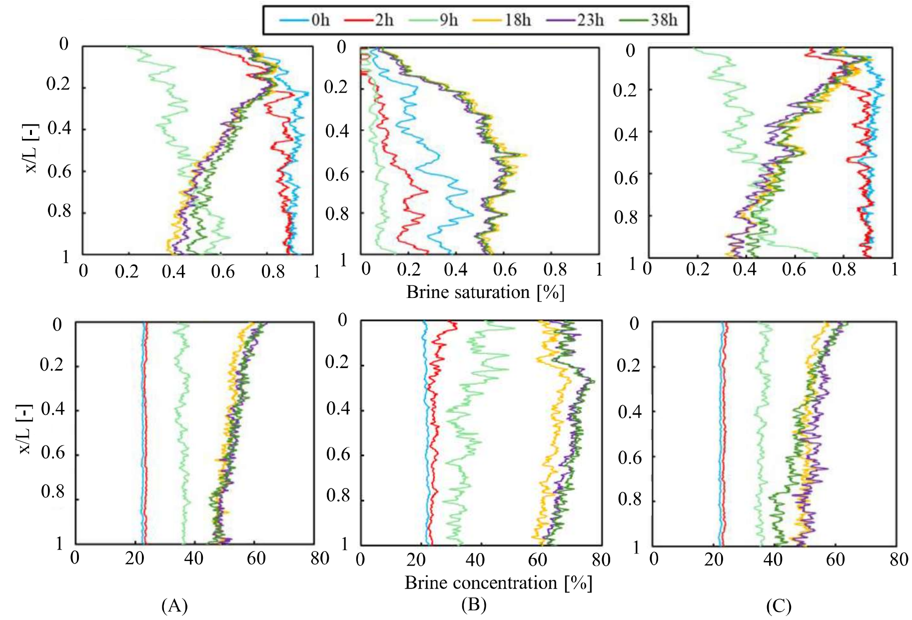

Fig. 4 Distribution of slice averaged salinity in a horizontal cross-section for three regions

Quantitative results, shown in Fig. 4, reveal that the initial brine saturation was slightly higher at the bottom of the fracture zone (0.4), while it was only 0.1 near the inlet. As gas was injected, brine saturation decreased significantly in the fractured zone, while in the matrix pores, brine reduction was observed primarily at the top. After 9 hours of injection, brine saturation dropped significantly in the matrix pores, ranging from 0.2 to 0.6 on both sides. In the fracture zone, brine saturation only slightly decreased, mainly due to depletion at the top. After 18 hours, salt accumulated in the fracture zone, with the maximum porosity reduction of 52% at x = 0.5. Capillary backflow was measured based on the salt location in the porous media system. Up until 9 hours of injection, capillary backflow did not appear, likely because gas saturation was not high enough to create a pressure gradient. As water saturation decreased in the matrix pores, capillary backflow emerged and caused salt accumulation in the fracture zone.

This study presents insights into the evaporation and capillary backflow dynamics in fracture porous media, highlighting the influence of gas and brine saturation on the evolution of salt accumulation. The findings demonstrate that as gas penetrates the fracture zone, brine saturation decreases, leading to salt precipitation and porosity reduction in the fracture. Additionally, the development of capillary backflow becomes evident once gas saturation reaches a certain threshold, which further influences the salt distribution and accumulation patterns in the system.

Conclusions

This study provides valuable insights into the effects of evaporation and gas penetration on brine evaporation and salt accumulation within fractured porous media. The results highlight how the distribution of gas and brine saturations influences the spatial dynamics of salt precipitation, with significant porosity reduction occurring in the fracture zones. As gas penetrates and displaces brine, the brine saturation decreases, and salt begins to accumulate, leading to porosity reduction in the fracture zone. Capillary backflow emerges after a certain threshold of gas saturation, further affecting the movement of fluids and salt distribution. These findings emphasize the complex interplay between gas injection, brine saturation, and capillary forces in controlling the behavior of fluid flow and salt precipitation in fractured porous media.

Future studies should focus on clarifying the effects of the spatial distribution of salt on the permeability of porous media. Understanding how salt accumulates in different regions of the porous medium and its impact on the flow pathways can help refine models of fluid and solute transport in fractured systems. Specifically, research could investigate the changes in permeability as salt deposits alter the connectivity and flow characteristics of the pore network. Additionally, exploring different environmental conditions, such as varying gas injection rates, brine concentrations, and porous media types, would provide deeper insights into the mechanisms that control permeability changes in systems undergoing evaporation and salt precipitation.

References

[1] P. Fu, R.R. Settgast, Y. Hao, J.P. Morris, F.J. Ryerson, The Influence of Hydraulic Fracturing on Carbon Storage Performance, J. Geophys. Res. Solid Earth 122 (2017) 9931–9949. https://doi.org/10.1002/2017JB014942.
[2] S. Jung, K. Lee, Effects of aquifer size and formation fracture pressure on CO2 geological storage capacity, Front. Energy Res. 12 (2024) 1–13. https://doi.org/10.3389/fenrg.2024.1381402.
[3] D. He, R. Xu, T. Ji, P. Jiang, Experimental investigation of the mechanism of salt precipitation in the fracture during CO2 geological sequestration, Int. J. Greenh. Gas Control 118 (2022). https://doi.org/10.1016/j.ijggc.2022.103693.
[4] S. Vialle, J.L. Druhan, K. Maher, Multi-phase flow simulation of CO2 leakage through a fractured caprock in response to mitigation strategies, Int. J. Greenh. Gas Control 44 (2016) 11–25. https://doi.org/10.1016/j.ijggc.2015.10.007.
[5] A.M. Norouzi, M. Babaei, W.S. Han, K.Y. Kim, V. Niasar, CO2-plume geothermal processes: A parametric study of salt precipitation influenced by capillary-driven backflow, Chem. Eng. J. 425 (2021). https://doi.org/10.1016/j.cej.2021.130031.
[6] S.M. Roels, N. El Chatib, C. Nicolaides, P.L.J. Zitha, Capillary-Driven Transport of Dissolved Salt to the Drying Zone During CO2Injection in Homogeneous and Layered Porous Media, Transp. Porous Media 111 (2016) 411–424. https://doi.org/10.1007/s11242-015-0601-y.
[7] D. He, P. Jiang, R. Xu, Pore-Scale Experimental Investigation of the Effect of Supercritical CO2 Injection Rate and Surface Wettability on Salt Precipitation, Environ. Sci. Technol. 53 (2019) 14744–14751. https://doi.org/10.1021/acs.est.9b03323.
[8] H. Ott, S.M. Roels, K. de Kloe, Salt precipitation due to supercritical gas injection: I. Capillary-driven flow in unimodal sandstone, Int. J. Greenh. Gas Control 43 (2015) 247–255. https://doi.org/10.1016/j.ijggc.2015.01.005.
[9] K. Pruess, N. Müller, Formation dry-out from co2 injection into saline aquifers: 1. effects of solids precipitation and their mitigation, Water Resour. Res. 45 (2009). https://doi.org/10.1029/2008WR007101.
[10] D. Akindipe, S. Saraji, M. Piri, Salt precipitation during geological sequestration of supercritical CO2 in saline aquifers: A pore-scale experimental investigation, Adv. Water Resour. 155 (2021). https://doi.org/10.1016/j.advwatres.2021.104011.
[11] M. Nasir, K. Kaito, A. Patmonoaji, M.A. Mahardika, Y. She, S. Matsushita, T. Suekane, Three-dimensional pore-scale observation of drying process of porous media, Int. J. Heat Mass Transf. 196 (2022). https://doi.org/10.1016/j.ijheatmasstransfer.2022.123299.
[12] S. Bakhshian, S.A. Hosseini, Pore–scale analysis of supercritical CO 2 –brine immiscible displacement under fractional–wettability conditions, Adv. Water Resour. 126 (2019) 96–107. https://doi.org/10.1016/j.advwatres.2019.02.008.
[13] A. Patmonoaji, M.A. Mahardika, M. Nasir, Y. She, W. Wang, M.A. Muflikhun, T. Suekane, Stereolithography 3D Printer for Micromodel Fabrications with Comprehensive Accuracy Evaluation by Using Microtomography, Geosci. 12 (2022). https://doi.org/10.3390/geosciences12050183.